Civil Engineering Infrastructures Journal xx,xx

DOI: 10.22059/ceij.2026.396108.2320

Enhancing the Compression Ductility of Masonry Assemblies Using Self-Reinforced Concrete Blocks

Masoomeh Bahrami[1], Hamid Toopchi-Nezhad[1,*], Reza Aghayari[1], and Mehrzad Tahamoliroodsari[2]

[1] Department of Civil Engineering, Razi University, Kermanshah, 67149-67346, Iran.
[2]Department of Civil Engineering, Islamic Azad University, Kermanshah Branch, Kermanshah, Iran.
* Corresponding Author, h.toopchinezhad@razi.ac.ir

Received: 26/05/2025

Revised: 13/11/2025

Accepted: 30/12/2025

ABSTRACT

Ductile masonry designs often require complex detailing, leading to higher construction and inspection costs. The primary objective of this study was to examine the performance of an innovative ductile masonry assembly employing self-reinforced (SR) concrete blocks. The SR blocks comprise two hollow circular cells, each reinforced with an internal spiral to provide lateral confinement for both the grouted block cell and enclosed portion of the masonry block. The SR blocks have the same overall dimensions as conventional masonry units and can be laid on a reinforced concrete masonry structure without incurring additional costs. In this study, the stress-strain behavior of half-scale masonry prisms constructed with self-reinforced (SR) blocks was evaluated and compared to that of conventional prisms used as references. The test results revealed that the SR blocks significantly improved the performance of the masonry prisms under compression, retaining approximately 80% of their initial peak capacity up to a compressive strain of 2%. The strain ductility and modulus of toughness were 5.2 and 7.9 times the values obtained for the reference prisms, respectively. Two analytical models for predicting the ultimate strength and strain of confined concrete were examined and found not to be sufficiently accurate for confined masonry using SR-blocks.

keywords: self-reinforced concrete block; confined masonry prisms; spiral confinement; strain ductility; modulus of toughness; ductile structural system

1. INTRODUCTION

Masonry shear walls can effectively withstand both gravitational and lateral loads. These walls serve various additional purposes in masonry buildings, including dividing spaces, providing thermal and acoustic insulation, and providing fire protection. Masonry buildings offer several advantages, such as the ability to utilize local labor and materials, ease of construction, long-term durability, aesthetic appeal, and cost-effectiveness. Owing to these advantages, masonry structures have been widely adopted as common structural systems in various regions worldwide (Drysdale. (2005)). According to most design codes, the use of reinforced masonry structures has been restricted to high-seismic-hazard areas owing to their limited ductility. Consequently, masonry buildings in such regions have been unable to compete with other contemporary structural systems such as reinforced concrete and steel structures (Drysdale. (2005)).

Masonry prisms, composed of units, mortar, and grout, can be used to experimentally evaluate the response behavior of a masonry assemblage under compression, tension, shear, and flexure (Raposo. (2018)). Toe crushing is a common failure mode in flexural masonry shear walls during earthquakes (Kanani, et al. (2023)). This is a form of compression failure that occurs in masonry materials. Vertical compression testing of masonry prisms is typically conducted to assess the response behavior of masonry under compression. Research indicates that a fully grouted masonry prism under a concentric compression load typically fails owing to the vertical splitting of the concrete masonry units caused by the lateral expansion of the mortar and grout. This results in an early deterioration of the load-carrying capacity at strain values less than 0.004 (Al-Ahdal, et al (2025)). Up to this strain level, the load is shared between the grout and masonry units based on their stiffness values. However, for larger strain values, the ability of the section to resist continued loading will depend on the compression capacity of the grouted cell.

The utilization of lateral confinement to enhance the load and deformation capacity of materials to withstand axial compression is a well-understood mechanism. During axial compression, the lateral expansion of the material creates pressure against the confining device, leading to the development of circumferential reaction stress known as the confining pressure. This confining pressure counteracts the lateral expansion and induces a state of triaxial compression, significantly increasing the ability of the material to resist vertical axial loads by improving its crushing strain. Depending on the level of confinement, the resistance to axial load can be several times higher than that in the case of uniaxial compression (Mander, et al (1988)). More recent experimental and numerical studies have demonstrated that modern confinement techniques, including fiber-based and hybrid confinement systems, significantly enhance the axial strength, deformation capacity, and post-peak ductility of masonry components under compression loading (Niazi et al., 2025).

An early technique for confining masonry assemblages was the Bed Joint Confinement Technique, proposed by Priestly and Bridgeman in 1974. This method involves placing a confinement within the mortar bed joint to provide lateral support for the concrete block and prevent its tendency to split. A 3 mm thick stainless (or galvanized) steel plate with dimensions matching the block size was used to limit the lateral expansion of the mortar bed joint. This restriction decreases the natural lateral expansion and vertical splitting of the masonry block under vertical compression. Additionally, it provides support against the buckling of the vertical compression steel inside the

grouted block cells. Hart et al. studied different types of bed joint reinforcements, such as closed wire mesh and open wire mesh (confining comb). Their experiments showed that all the confinement techniques investigated moderately improved the drift capacity and energy absorption of the masonry shear walls. An important consideration in the effectiveness of a confinement device embedded in a mortar bed joint is the spacing of the bed joints, which is determined by the height of the masonry block. Snook incorporated three different types of bed joint confinement techniques (steel plates, steel confinement combs, and fiber wraps) into large-scale reinforced masonry shear walls and concluded that adding fiber wraps can significantly enhance the performance of the walls (snook, (2005)).

In-cell confinement is another technique used to improve the compression behavior of masonry assemblages. This method involves placement of a confinement device within the grouted cells of the concrete block. Hart et al. compared four different in-cell confinement techniques, including ties, cage (hoop), spiral, and cage (spiral). With these techniques, over 50% of the wall cross-sectional area remained unconfined and was subjected to spalling under compressive loads. Additionally, in typical running-bond construction with standard concrete blocks, the block cells did not align from course to course. This misalignment forced the in-cell confined grout to be offset from course to course, preventing the formation of a fully continuous column of confined grout (Hart et al (1988)). Another type of in-cell confinement involves reinforcing grout with fibers. In a study conducted by Gouda et al. (2020), a set of 36 fully grouted half-scale masonry prisms with varying glass fiber ratios was investigated. The findings revealed that the addition of glass fibers to the grout significantly enhanced the compressive strength of the masonry prisms at higher fiber percentages (0.10%). Specifically, the increase in the compressive strength was approximately 9.8% for the high-strength two-block high specimens, 10.1% for the normal-strength two-block high specimens, and 39% for the normal-strength five-block high specimens. Hervillard et al. (2005) found that the use of polymer fibers (synthetic fibers made of two types of polymers: polypropylene and polyethylene) mixed into the grout in concrete masonry is effective at increasing the strain capacity at peak stress and at 50% of peak stress, but the results were highly dependent on the amount of fibres present in the grout mix. In another experimental study, concrete masonry block walls with grouted cores, vertical reinforcement, and spiral confinement in the grouted cores were examined. The test results suggest that the lateral confinement of the core has a positive effect on the post-peak ductility (Paturova. A (2006)).

The addition of boundary elements at the ends of masonry shear walls has been shown to significantly improve their ductility and energy dissipation capabilities, as demonstrated in experimental studies conducted by Shedid, et al. (2010), Banting (2013), AbdelRahman, et al. (2022), Aly, N. et al (2019) , Dou, M. et al. (2022) and Albutainy, et al. (2024). These studies involved wall specimens with enlarged boundary elements, similar to pilasters constructed from fully grouted masonry units. The grouted cells at the boundary elements were confined by transverse steel reinforcement. The wall specimens were then subjected to fully reversed quasi-static load cycles. The boundary element is the key element for enhancing the performance of masonry walls.Abdolrahman et al. (2021) by investigating the axial monotonic compressive behavior of unconfined and confined RMBEs, proposed an monotonic and cyclic stress-strain models for confined and unconfined concrete-masonry boundary elements subjected to axial compression loading. Recent numerical investigations have shown that boundary and interface

conditions significantly influence masonry behavior, particularly by reducing initial stiffness while marginally affecting ultimate strength when gaps are present (Islam et al., 2024).

The various techniques discussed earlier for confining masonry walls involve detailed construction and inspection, which lead to increased project costs. Another recent method involves the use of self-reinforced (SR) concrete masonry blocks in critical regions of shear walls, which was initially proposed by Toopchi-Nezhad et al.(2011). The SR blocks, which are factory-made in a controlled manufacturing environment, have the same dimensions as conventional masonry units and can be laid on the wall without incurring additional costs. The use of confinement to improve the load resistance of materials is a well-understood mechanism, where the lateral expansion of the material during axial compression creates pressure against the confining device and causes it to develop circumferential confining stress. This provides resistance to the lateral expansion of the confined material and introduces lateral compression within the confined material so that it is in a state of triaxial compression, which significantly increases the ability to resist vertical axial load by increasing the crushing strain of the material. Depending on the amount of confinement, the resistance to axial loads may be several times higher than that of uniaxial compression (Joyal, et al. (2013)). A further benefit of confinement within these compression zones is to provide lateral support for the vertical reinforcement, delaying or preventing buckling of the reinforcement steel under compression. A summary of the in-cell confinement techniques is presented in Table 1.

Table 1 Summary of in-cell confinement techniques for concrete masonry

Confinement Technique	Scholars	Year	Observations
Ties- Cage (hoop)- Spiral - Cage (Spiral)	Hart et al.	1988	- Enhanced strength in the ascending portion of the stress-strain curve - Positive influence on post-peak ductility - Gradual failure in the confined systems - Occurrence of spalling in concrete blocks
Polypropylene and Polyethylene Fiber-reinforced grout	Hervillard et al.	2005	- Enhanced ascending branch of the stress-strain curve (improved strength and strain) - Minimal enhancement in post-peak ductility - Effectiveness of fiber addition varied with the quantity used - Transition from sudden failure to gradual failure with fiber addition - Occurrence of spalling in concrete blocks
Spiral confinement in the grouted cores	Paturova	2006	- Insignificant improvement in the ascending branch of the stress-strain curve - Positive influence on post-peak ductility - Relatively ductile failure mode - Occurrence of spalling in concrete blocks
Self-reinforced concrete block	Toopchi-Nezhad et al.	2011	- Enhanced strength in the ascending portion of the stress-strain curve - Improved post-peak ductility
	Joyal et al.	2014	- Ductile failure mode - Occurrence of spalling in the block shell
Glass fiber-reinforced grout	Gouda et al.	2020	- Enhanced ascending branch of the stress-strain curve (improved strength) - Insignificant enhancement in post-peak ductility - Effectiveness of fiber addition varied with the quantity used

	- Transition from sudden failure to gradual failure with fiber addition - Occurrence of spalling in concrete blocks

Testing full-scale masonry specimens and systems is expensive. Recent experimental studies have shown that quasi-static testing of half-scale masonry structures, when designed based on geometric and material similitude principles, can reliably capture the strength and deformation characteristics of full-scale masonry systems (Aşıkoğlu et al., 2025).The use of model-scale specimens and structures is a cost-effective approach for experimental studies. In a study conducted by Kahrizi et al. (2022), researchers examined the impact of scaling on the mechanical properties of concrete blocks and prisms. When testing a model scale of a prototype, the similitude law requirements ensure that the model accurately represents the behavior of the full-scale prototype (Harris, et al. (1999)). To achieve representative results, the key requirements in pseudo-static testing of half-scale masonry prisms include satisfying both geometric and material similarities. To achieve geometric similarity, the maximum size of aggregates in the concrete, mortar, and grout mixes, the physical dimensions of the blocks, and the dimensions of the mortar joints were scaled down by a factor of 2. This ensured that all linear dimensions of the model were proportional to the corresponding dimensions of the prototype. Additionally, the cement and aggregate materials used in the half-scale prisms had similar properties to those used in the prototype. Kahrizi et al. (2022) indicated that the response of standard half-scale specimens, which satisfy similitude law requirements, can be reliably extended to full-scale masonry.

The main objective of this study is to examine the performance of novel self-reinforced (SR) concrete masonry blocks in enhancing the ultimate strength, toughness, and strain-ductility of masonry prisms under compressive loads. To achieve this, two sets of half-scale, fully-grouted masonry prisms were constructed. The principles of similitude law, as outlined previously, were followed in constructing the half-scale prisms. Set 1, which employed conventional stretcher concrete masonry blocks, is termed unconfined prisms (UPs) and served as reference specimens. Set 2 included confined prisms (CPs) constructed using SR-blocks. The final component of the study involves assessing the accuracy of two distinct analytical models in evaluating the compressive strength of the confined prisms, based on the ultimate strength of the reference prisms and the level of confinement pressure provided. To the authors' best knowledge, no similar study exists in the literature.

2. TEST PROGRAM

The test program in this study included evaluating the compressive strength of ½ scale mortar cement and grout specimens. Additionally, the experimental stress-strain behavior of the masonry prisms under compression was evaluated to assess the influence of the confinement provided by the SR-blocks on the load-bearing and deformation capacity of the prisms. Half-scale masonry assemblages were used in this study because of their convenience of operation and cost-effectiveness. These assemblages were designed and constructed according to the similitude law (Harris, et al. (1999)), ensuring that the material and geometrical properties of the model accurately represented those of the full scale. The physical dimensions of the model-scale block and its granular aggregates are multiplied by a factor of ½. The same mix design as outlined in the work by Kahrizi et al. was used for the half-scale masonry assemblages in this study. To achieve a well-

graded half-scale aggregate consistent with full-scale granular materials, the sieve sizes of the upper and lower bounds of ASTM C136 were multiplied by a scale factor of ½.

The provisions of CSA S304.1 were followed to evaluate the experimental stress-strain behavior of masonry prisms under compression. Annex D of this standard provides the requirements for the test specimens, test procedure, compressive strength evaluation, and test report. The test method is similar in many aspects to the provisions of ASTM C1314; however, according to CSA, the test prisms must comprise four courses of concrete blocks, three rows of mortar bed joints, and two mortar head joints.

Figure 1 provides an overview of the testing machine used to evaluate the stress-strain behavior of the masonry prisms under compression. The universal test machine employed for this purpose was manufactured by Schenck RoTec GmbH, Germany, with a payload capacity of 600 kN. Equipped with both an inbuilt load cell and an LVDT (see Figure 1), the machine was capable of applying axial loads under displacement control using its inbuilt controller.

Figure 1 also includes a close-up view of one of the masonry prisms situated between the top and bottom platens. Each masonry prism had level surfaces at its top and bottom, which were already capped with high-strength gypsum. These leveled surfaces allowed for perfect vertical alignment of the prism. The prism was centered with the top and bottom platens of the test apparatus to ensure concentric axial loading. The upper platen was stationary, and the compressive axial loads were applied to the prism through the upward movements of the lower platen, controlled via the inbuilt controller of the test apparatus.

After positioning the prism in the test machine, it was subjected to vertical compression as the bottom head of the test machine moved upward at a prescribed rate. A loading rate of 0.006 mm/s was adopted up to an axial strain of approximately 0.002. Then, the loading rate was decreased to 0.002 mm/s to capture the post-peak behavior of the prisms more accurately. The loading continued until the post-peak compressive stresses decreased by approximately 40% of the peak resistance of the prism. The nominal stress-strain values were traced in real-time via the data logger that collected data at a rate of 2 Hz. The strain values were calculated by dividing the readings of the inbuilt LVDT of the test machine by the initial height of the prism, neglecting the capping deformation due to its limited thickness and high compressive strength. The initial height was measured for each of the masonry prisms before the application of vertical loads. The nominal stresses were evaluated by dividing the applied load by the original cross-sectional area of the prism, which was measured for each individual prism before testing was initiated.

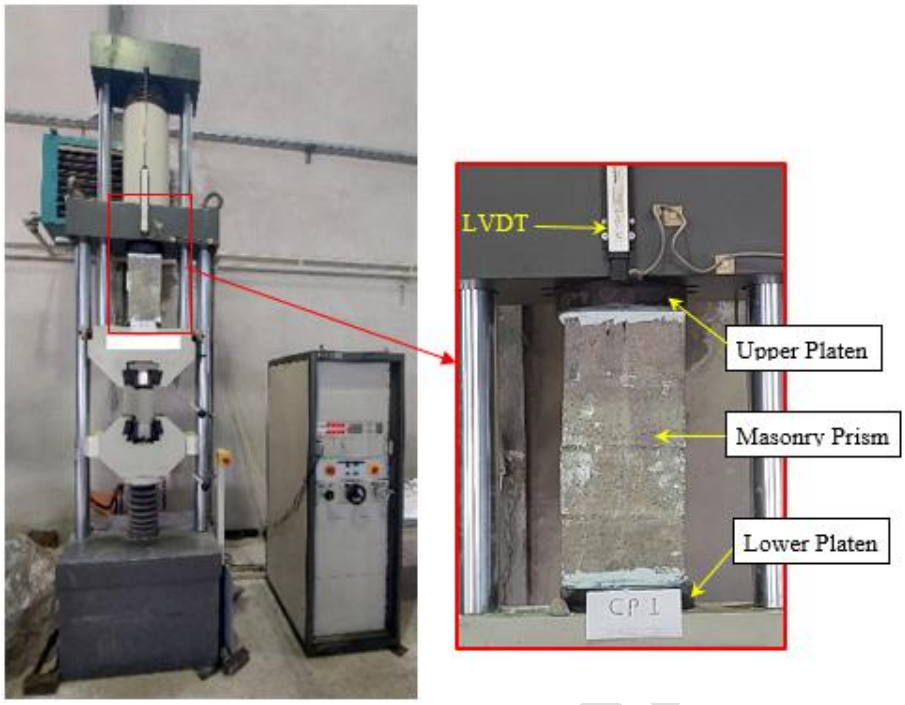

Fig 1. Test apparatus for testing the masonry prisms under axial compression

3. SPECIFICATIONS of MATERIALS and SPECIMENS

3.1. Masonry units

Figure 2 shows the half-scale hollow concrete masonry units used in this study. Figure 2a shows a conventional stretcher block, whereas Figure 2b shows a self-reinforced (SR) concrete block with two circular hollow cells. Each SR block was reinforced using two individual spiral reinforcement cages, each surrounding one of the two block cells, to provide lateral confinement to the grouted cells. Circular cell geometry was chosen to maximize the confinement effect provided by the spiral reinforcement. The conventional masonry unit was a half-scale replica of 20 cm masonry concrete blocks. The overall dimensions of the two masonry unit types are identical. Table 2 provides additional information on the geometric characteristics of masonry units. The physical dimensions, including the face shell and web thicknesses, met the minimum requirements outlined in ASTM C90.

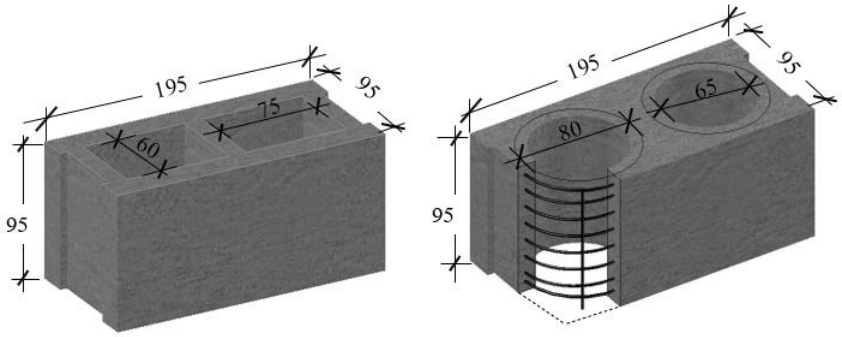

(a) (b)

Fig 2. Typical half-scale concrete masonry blocks (all dimensions in mm); a) Conventinal stretcher unit, b) Self-reinforced (SR) unit

Table 2 Physical dimensions of concrete masonry blocks

Specimen	Length (mm)	Heigth (mm)	Width (mm)	Face Shell Thickness (mm)	Web Thickness (mm)	Solid %
SR-Block	195	95	95	1.7	1.25	64
Standard Block						53

The half-scale concrete blocks were manufactured using a manual block-making machine specifically designed and fabricated for this research study. The machine can manufacture four concrete blocks at a time. The concrete, mixed using an electric mixer, is poured into the mold and compacted with vibration and pressure. Figure 3 provides an overview of the machine and illustrates how the spirals were positioned from the bottom into the mold. Two different sets of steel molds were fabricated for the individual manufacturing of the conventional and SR blocks. The figure also includes photographs of typical unmolded blocks.

(a) (b)

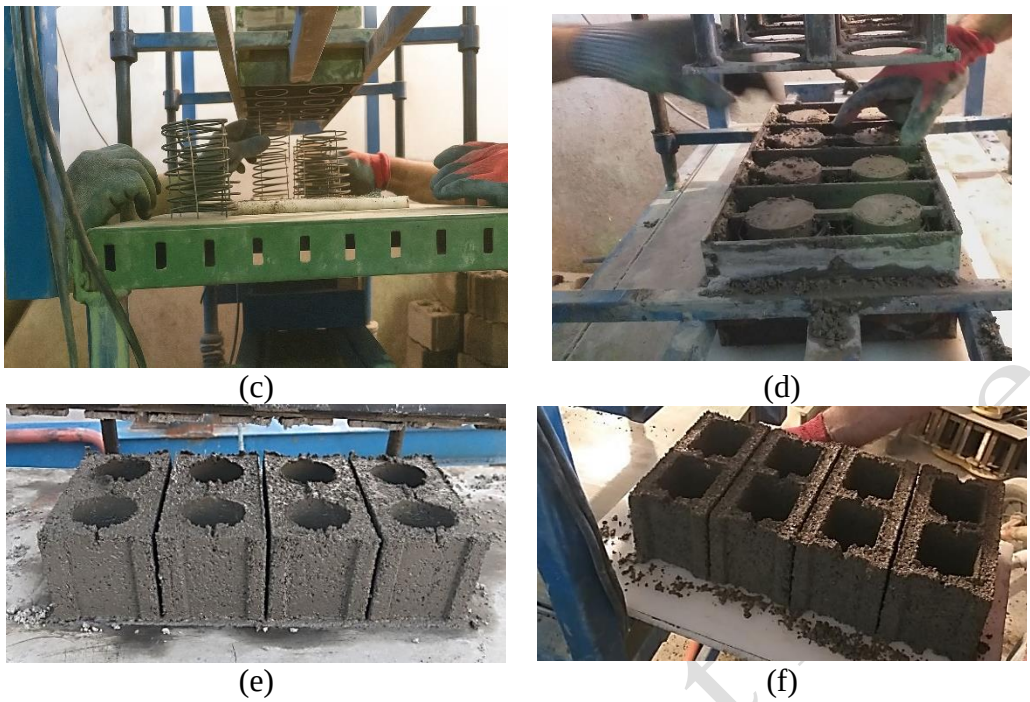

Fig 3. Fabrication of half-scale concrete masonry blocks; a) Overview of the manual block-making machine, b) Unloading the mold, c) Positioning the spirals into the mold, d) Mold with spirals inside, ready for pouring concrete, e) A set of four SR-blocks unmolded, and f) A set of four conventional blocks unmolded.

To ensure consistency, all the masonry blocks used in this study were fabricated in the same production run with the same concrete batch. The exact dimensions of each masonry unit were measured before testing. The top and bottom faces of the units were capped with high-strength gypsum in conformance with ASTM-C1552. Compressive tests were conducted on 28 days units. Table 3 lists the compressive strength values obtained for each test specimen. The average compressive strength was found to be 16.9 MPa and 17.6 MPa for the conventional and SR blocks, respectively. According to ASTM C90, the minimum expected compressive strength of the concrete masonry units should be approximately 14 MPa (2000 psi). Concrete masonry units are typically manufactured at strength values that are 20–30% greater than the minimum value specified above. The proximity of the average compressive strength values of the two masonry block types indicates that the influence of the internal reinforcement on the compressive strength of the ungrouted units is negligible. The coefficient of variation (COV) for the masonry units was found to be less than 15%. This level of consistency is generally considered acceptable in engineering and quality control, as it implies that the material properties are uniform and predictable.

Table3 Compressive strength of masonry units

Block type	Specimen	Failure load (kN)	Compressive strength (MPa)	Average strength (MPa)	COV%
Standard-Block	1	175	17.8	16.9	5.5
	2	168	17.1		
	3	156	15.9		
Self-reinforced Block	1	220	18.6	17.6	10.8
	2	190	16.0		

	3	215	18.1

3.2. Mortar and grout

In addition to the masonry units, mortar cement and grout are the two main components of masonry prisms. The sand grading for the preparation of mortar (Type S) and grout was based on ASTM C144 and ASTM C404 requirements, respectively. In the construction of the half-scale units, both the physical geometry of the concrete block and the maximum size of its coarse aggregate were multiplied by a scale factor of ½. The maximum size of the coarse aggregate in the mortar mix of the half-scale units was consistently divided by 2. For the full-scale units, sand material passing sieve #8 was employed in the mortar mix design in conformance with ASTM C270. Therefore, to construct a consistent mortar mix for the half-scale units, sand material passing sieve #16 was utilized.

The compressive test results for the mortar and grout specimens are presented in Tables 4 and 5, respectively. The average strengths of the mortar and grout specimens were found to be 14.4 MPa and 16 MPa, respectively. These values are deemed acceptable as they exceed the minimum requirements prescribed by standards such as ASTM C270, ASTM C476, and CSA A179. The COV for all mortar and grout specimens was found to be less than 15%, indicating suitability.

Table 4 Compressive strength of half-scale mortar specimens

Sample	Failure load (kN)	Compressive Strength (MPa)
1	36.3	14.5
2	34.8	13.9
3	37.3	14.9
Average	36.1	14.4
COV%		3.5

Table 5 Compressive strength of half-scale grout specimens

Sample	Failure load (kN)	Compressive Strength (MPa)
1	42.0	16.8
2	36.5	14.6
3	41.3	16.5
Average	39.9	16
COV%		7.5

3.3. Masonry prisms

Two sets of fully grouted masonry prisms were constructed in the laboratory using a professional mason at an ambient temperature of approximately 25 °C. Each set consisted of three specimens. The first set of prisms is fabricated using conventional concrete masonry blocks. The grouted cells in the specimens were unconfined. As such, these specimens were called unconfined prisms (UPs) and are referred to as reference prisms. The second set of specimens employed SR blocks, in which the grouted cells were confined by internal spirals. Therefore, they are termed as confined prisms

(CPs). Figure 4a shows sketches including the physical dimensions of the masonry prisms, which comprise four courses of concrete blocks, three rows of mortar bed joints, and two mortar head joints, as per the requirements of CSA S304.1. According to the Canadian Standard, this configuration is more representative because it accounts for the influence of multiple mortar joints, including both head and bed joints. Mortar joints significantly impact compressive strength due to their lower strength compared to masonry units. The thickness of the mortar joints in the half-scale prisms was approximately 5 mm. Figure 4b shows a photograph of the masonry prisms. As shown in this figure, the appearances of the confined and unconfined (reference) prisms are the same. According to ASTM-C1552 , the material used for capping masonry prisms must have a minimum compressive strength of 24 MPa after 2 hours. The prisms were capped with high-strength gypsum on the top and bottom surfaces before testing, with capping layers 2–3 mm thick (the permissible range by ASTM C1552). The prisms were tested 28 days after construction.

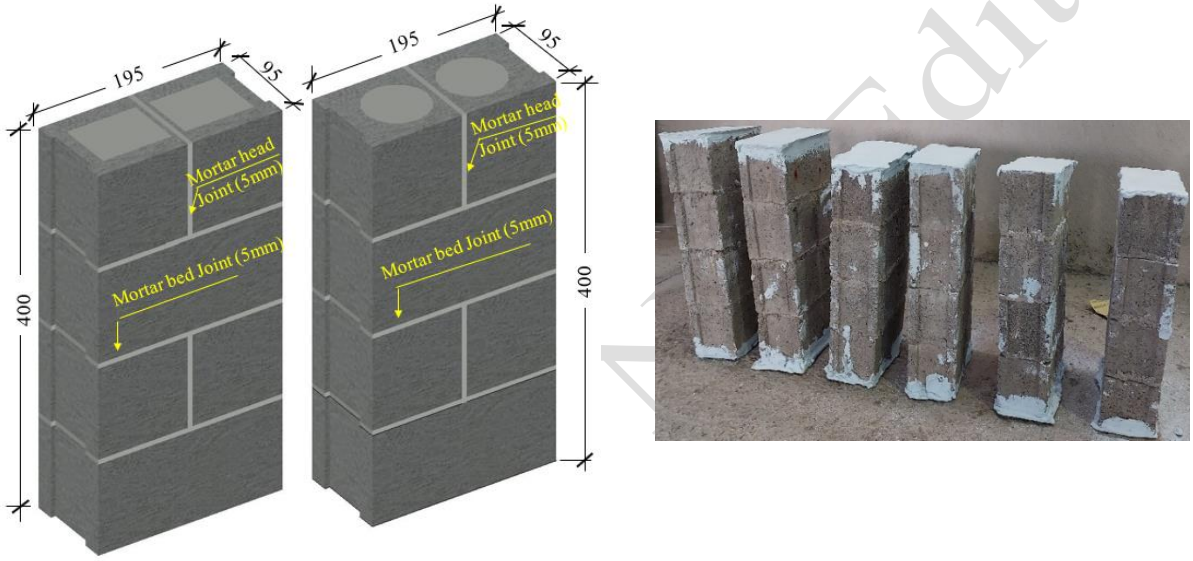

(a) (b)

Fig 4. Half-scale masonry prisms (confined and unconfined Prisms); a) Geometrical properties of prism (all dimensions in mm), b) Photograph of capped masonry prisms

4. TEST RESULTS ON MASONRY PRISMS AND DISCUSSION

4.1. Unconfined Prisms (UPs)

As previously stated, three fully grouted masonry prisms were constructed using conventional stretcher concrete blocks. The grouted cells in these prisms are unconfined, representing a standard practice for masonry construction. As such, they are termed as Unconfined Prisms (UPs). Figures 5a–5c show a close-up view of the failure mode observed in the UPs of this study. The failure was typically initiated by splitting of the concrete masonry blocks induced by the lateral expansion of the mortar and grout. No sign of distress was visible until the peak axial load.

Figure 6 shows the compressive stress-strain response of the UPs tested using the test apparatus shown in Figure 1. The peak strength achieved at a strain of approximately 0.002. The compression load capacity decreased owing to block failure, which was initiated by the gradual splitting of grouted cells and complete loss of capacity at strains slightly lower than 0.003. A fairly rapid decline in the compressive load capacity of the UPs following their peak strength indicates the brittle behavior of these prisms. Table 6 lists the ultimate compressive strength values of each

specimen. According to Table 6, the average strength of the UPs was found to be 13.9 MPa. Since the coefficient of variation (COV) was evaluated to be less than 15%, no additional prisms were needed to be tested as per Annex C of CSA S304.1 .

(a) (b) (c)

Fig 5. Failure modes in unconfined prisms (UPs); a) UP1, b) UPs, and c) UP3

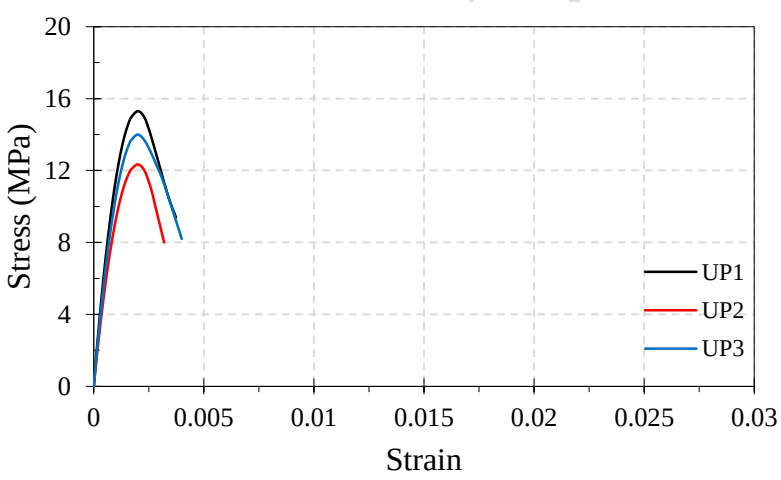

(a)

(b)

Fig 6. Performance of the unconfined prisms (UPs) under axial compression; a) Compression stress-strain curve, b) Typical failure pattern

Table 6 Test results for the unconfined prisms (UPs)

Prism	Failure load (kN)	Ultimate strength (MPa)
UP1	228.8	12.4
UP2	283.4	15.3
UP3	259.4	14.0
Average	257.2	13.9

COV%	10.5

4.2. Confined Prisms (CPs)

For this test series, three fully grouted masonry prisms were constructed using SR-blocks and denoted as confined prisms (CPs). The main purpose of internal reinforcement in an SR block is to provide lateral confinement for both the grouted cell and a portion of the block located inside the spiral reinforcement. The confining reinforcement provided resistance to the lateral expansion of the grout material and increased its ability to resist the vertical axial load by increasing the ultimate strain of the material under axial compression.

The damage initiation to failure of a typical CP specimen is shown in Figures 7a–7c. Figure 8a shows the compression stress-strain behavior of the confined prisms CP1 to CP3. Similar to the UP specimens, no visible signs of significant distress were observed in the specimens before the axial load reached its maximum value. Beyond the peak strength value, damage was initiated by the vertical splitting of the face shell of the concrete blocks, causing the concrete cover of the spirals to spall off (Figures 7a and 7b). The internal reinforcement (steel spiral), acting as a confining device, prevented the excessive lateral deformation of the grouted cells and significantly increased the ultimate compressive strain of the masonry prism to 0.02 or greater. The second peak of the stress-strain curve for each specimen is marked with a circle in Figure 8. Figure 7b, 7c, and 8b show the typical failure patterns observed in the CP specimens in this study. A close examination of these figures indicates that the unconfined concrete material between the two confined grouted cells of the prism is crushed. This occurred during the post-peak stage of the load-deformation curve. Consequently, the confined block cells function as two individual columns, effectively retaining a significant portion of the load-bearing capacity of the confined prism.

(a) Initial vertical compression splitting

(b) Spalling of concrete cover of spiral

(c) Typical failure pattern

Fig 7. Damage initiation and failure pattern of a typical Confined prism (CPs)

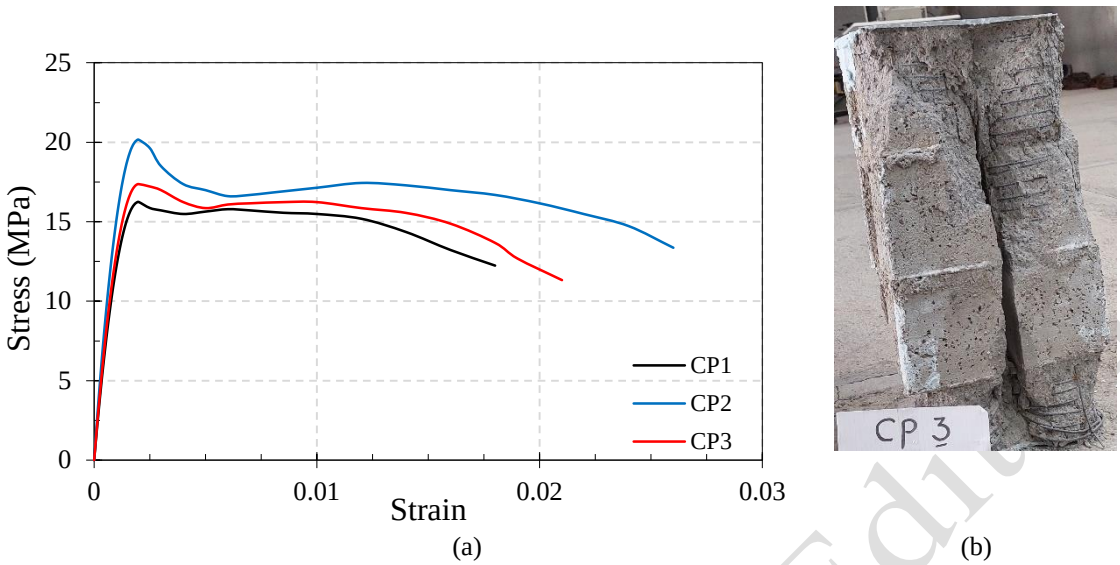

Fig 8. Performance of the confined prisms (CPs) under axial compression; a) Compression stress-strain curve, b) Typical failure pattern

Table 7 presents the test results for the confined prisms. The coefficient of variation (COV) for the CP specimens was approximately 11%, which was less than 15%. Thus, no additional prisms were tested as per Annex C of CSA S304.1.

Table 7 Test results for the confined prisms (CPs)

Prism	Failure load (kN)	Ultimate strength (MPa)	Modified strength* (MPa)
CP1	302	16.3	19.4
CP2	374.2	20.2	23.4
CP3	322.3	17.4	20
Average	332.8	18.0	20.9
COV%		11.1	

*Correction Factor (1.16) × Ultimate Strength

4.3. Discussion

This research study utilized concrete blocks, mortar, and grout made from the same material and manufactured consistently, ensuring similar block properties. This consistency was crucial for making direct comparisons between the different series of prism tests. The tests of the unconfined prisms and their individual components showed strengths consistent with previous research and the values published in the design standard (CSA S304.1(2014)). Consequently, there was a robust data foundation to evaluate the effect of using confining devices within concrete blocks.

The compressive stress-strain curves for both confined and unconfined masonry prisms are shown in Figure 9. The curves in Figure 9 represent the average data obtained for each prism type tested in this study. As can be seen in Figure 9, the average stress-strain curve of the CPs showed a relatively sharp post-peak falling branch, similar to what is typically seen in unconfined prisms, up to a stress decrease of approximately 12% of the peak stress. From this point on, the role of internal reinforcement in improving the ductility of prisms became more apparent as the prisms were capable of withstanding very large strains with no significant loss of load capacity. As seen in Figure 9, the internal reinforcement significantly flattened out the post-peak branch of the stress-

strain curve as very large strains (even more than 0.02 according to Figure 8) were achieved in the tested prisms. At a strain of 0.01, more than 85% of the maximum capacity was still retained.

According to Figure 9 the average peak compressive strength of the CPs was found to be approximately 29% greater than the average peak strength of the UP specimens. This increased strength is partially attributed to the reduced effect of the smaller volume of grout (Drysdale. (2005))., different geometry of the block cells, and the relatively higher average strength of the SR masonry units (see Table 3). The internal spirals each consist of three vertical rebars with a diameter of 2.5 mm. Given the insignificant cross-sectional area of the vertical steel, the role of internal reinforcement in increasing the peak strength response before the outer concrete shell spalls is minimal. In this study, the standard blocks had an average compressive strength of 16.9 MPa and were 53% solid. In comparison, the SR blocks had an average compressive strength of 17.6 MPa and were 64% solid. To scale the results to a common property, the compressive strength of the unconfined prisms can be adjusted by multiplying the solid ratio of 64/53 = 1.21 and the masonry unit strength ratio of 17.6/16.9 = 1.04. The resulting scale ratio of 1.21 × 1.04 = 1.25 is comparable to the average experimental CP to UP strength ratio of 1.29. However, accurately evaluating the CP to UP strength ratio is very challenging, as the simple assessment mentioned above ignores the complex relationship between block compressive strength, cell geometry, and the volume of grout in the prism.

The peak compressive strength of the CP specimens occurred at an average compressive strain of 0.0024. A significant decrease in the load carrying capacity of the CP specimens after the peak load was reached can be attributed to the significant loss (46%) in the original cross section area due to spalling of the outer concrete shell. However, unlike what is expected for a laterally confined spirally reinforced concrete column (Mander, et al (1988)). no significant after-spalling increase in the load carrying capacity was observed for the CP specimens. In reinforced concrete columns, the typical 20% loss of area due to spalling can be offset by increased strength of the confined area as increased axial compression strain causes the confining effect of the spiral reinforcement to increase. Clearly, in the case of the CP specimens, the amount of confinement produced was not sufficient to increase the vertical compressive strength sufficiently to offset the 46% loss of cross section area. Nonetheless, the confining device was effective in producing increased compressive strength of the confined core so that a very gradual decrease in capacity was observed.
Overall, the stress-strain curves obtained in this study for the CP specimens are similar to those from an experimental proof-of-concept study conducted on full-scale half-block confined masonry prisms, which led to a patent application (Toopchi-Nezhad et al.(2011)). In an experimental study by Joyal et al. (2013) on full-scale confined masonry prisms, the stress-strain curve, after its initial peak at a strain of approximately 0.002, exhibited a sharp decline up to a stress decrease of about 8%. From this point, the confining effect of the internal reinforcement came into play, resulting in a positive load-bearing capacity. A second peak, with approximately a 5% increase over the initial peak at a strain of nearly 0.012, was observed, beyond which the stress-strain curve gradually declined. Clearly, the amount of confinement produced was sufficient to increase the vertical compressive strength enough to offset the loss of cross-sectional area. The confinement pressure provided in the confined prisms of Ref. (Joyal, et al. (2013)) was approximately 4.8 MPa, nearly three times larger than the 1.6 MPa provided for the confined prisms in this study. The calculation of confinement pressure has been provided in Section 5 of this paper.

At the ultimate stage of the test on the CP specimens, shear sliding between the confined columns of grouted cells resulted in significant damage and capacity degradation. A potential solution to

this issue is to provide bed joint reinforcement, which can improve performance by increasing resistance to shear sliding and preventing the columns of grouted cells from acting independently. The strain-ductility supply can be evaluated by dividing the ultimate strain by the nominal yield strain of the prism. The nominal yield stress and strain values of the prisms were evaluated using the offset method (Gouda, et al. (2020)). In the post-peak branch of the stress-strain curve, the strain corresponding to a 20% reduction in the peak lateral load resistance was used to evaluate the ultimate strain of the prisms. This 20% strength reduction is typically considered the limit for strength loss due to seismic damage to the wall. The average strain ductility of the CP specimens was calculated to be 18.3, which is 5.2 times higher than the average value calculated for the reference UP specimens. The modulus of toughness is another important parameter that indicates the energy-absorption capability of a material. By definition, the modulus of rupture represents the ability of a material to absorb energy before fracture. The area below the stress-strain curve represents this energy. On average, the modulus of toughness of the CP specimens was found to be 7.9 times greater than that of the reference UP specimens. The strain ductility ratio and toughness modulus of the prisms are listed in Table 8. This section highlights the significant impact of the SR blocks on the mechanical properties and deformation characteristics of concrete masonry prisms subjected to compressive loads.

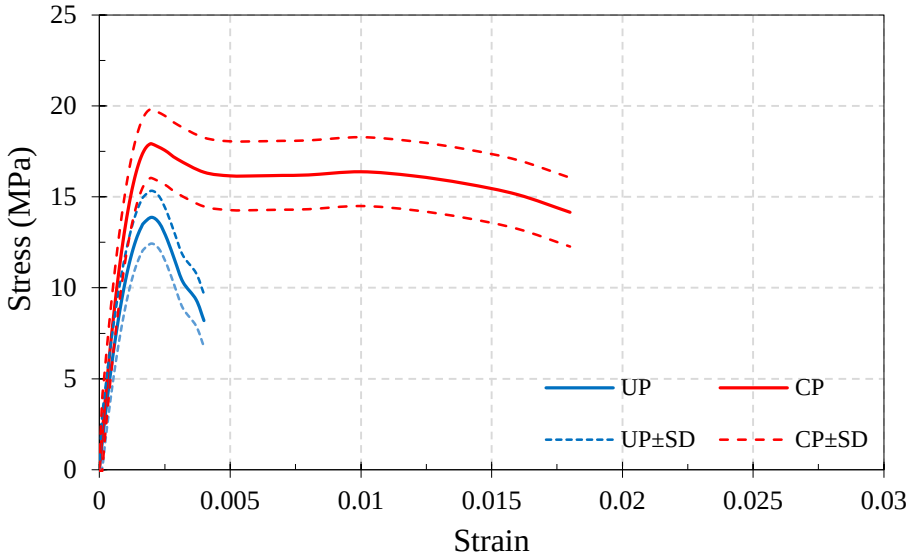

Fig 9. Average stress-strain curves for unconfined and confined prisms

Table 8 Strain ductility ratio and Modulus of toughness

Specimen	ε_y	$\varepsilon_{\text{at peak stress}}$	$\varepsilon_{ultimate}$	strain-ductility $\frac{\varepsilon_{ultimate}}{\varepsilon_y}$	strain-ductility $\frac{\varepsilon_{ultimate}}{\varepsilon_{\text{at peak stress}}}$	Modulus of toughness (MPa)
UP1	0.0011	0.0021	0.0041	3.7	1.95	0.046
UP2	0.0012	0.002	0.0033	2.7	1.7	0.03
UP3	0.0012	0.0022	0.0043	3.58	1.95	0.044
Average of UPs	0.0012	0.002	0.0042	3.5	2.1	0.042
CP1	0.0012	0.0022	0.018	15	8.2	0.26
CP2	0.0013	0.0023	0.026	20	11.3	0.42
CP3	0.0012	0.002	0.021	17.5	10.5	0.32
Average of CPs	0.0012	0.0022	0.022	18.3	10	0.33

4.4. Potential application of SR-blocks

A potential application for SR-blocks is their use in the critical regions of reinforced masonry shear walls to enhance curvature ductility. The current code-oriented approach to enhancing the curvature ductility of reinforced masonry shear walls involves incorporating boundary elements. CSA S304.1 and offer guidelines for the design of ductile shear walls with boundary elements. Alternatively, some design codes, such as NZS 4230, provide guidelines for the inclusion of horizontal confining plates in ductile masonry shear walls. According to NZS, the confining plates effectively increase the maximum masonry compressive strain in the plastic hinge regions of rectangular shear walls to as high as 0.008, which aligns with the value specified by CSA S304.1 for shear walls with boundary elements. To conclude, the current code-based approach to designing ductile masonry shear walls includes relying on the improved strain ductility of the masonry assemblage at the critical plastic hinge regions. SR-blocks provide a similar technical advantage by significantly enhancing the ultimate compression strain of the masonry.

5. ANALYTICAL EVALUATIONS

This section addresses the analytical evaluation of the post-peak ultimate compressive strength of the confined masonry prisms and their corresponding longitudinal strain. Two different analytical models have been employed to estimate the compressive strength of the confined masonry. The compressive strength of confined masonry is influenced by the unconfined specific compressive strength of the materia (f'_m), and the level of confining pressure applied to the masonry assemblage. The parameter (f'_m) , based on an available set of experimental data, can be determined following a code-based approach, as discussed in the next section.

5.1. Specific Compressive Strength of Unconfined Prisms

Compressive strength is a fundamental design parameter for masonry structures. Other design parameters, such as the effective Young's Modulus, E_m, and the ultimate strain, ε_{mu}, are influenced by the compressive strength of the masonry assemblage. Accurate evaluation of these parameters allows for a reasonable prediction of the stress-strain behavior of the masonry assemblage. The specific compressive strength of masonry prisms can be evaluated based on the provisions of standards such as CSA S304.1 or ASTM C1314. In this study, the provisions of CSA S304.1 have been taken into account.

According to CSA S304.1 [24], the specific compressive strength, f'_m, of a masonry prism can be determined using Equation (1).

$$f'_m = f_{av} - 1.64S \quad (1)$$

where, f_{av} represents the average compressive strength of the test specimens, and *S* reflects the standard deviation of the data.

The compressive strength values should be modified by a correction factor to account for the height-to-thickness (*h/t*) aspect ratio of pisms. Given the aspect ratio of 4.2 of the prisms in this study, the correction factor based on Annex D of CSA S304.1 was evaluated to be of 0.96. Table 9 presents the experimental compressive strength values, the values adjusted for the aspect ratio, and the specific compressive strength values, f'_m, estimated for the conventional (unconfined) prisms based on CSA S304.1 [24].

Table 9 Specific compressive strength, f'_m (MPa), of conventional (unconfined) masonry prisms

Prism	Experimental Values	CSA S304.1 [22]	
		Adjusted Values*	f'_m
UP1	12.4	11.9	
UP2	15.3	14.7	11.1
UP3	14.0	13.4	
f_{av}	13.9	13.3	
S	1.45	1.39	

* Adjusted for the aspect ratio (h/t) of prisms
f_{av} = Average experimental compressive strength
S = Standard deviation of data

5.2. Evaluation of Confined Prisms

The test results indicate that the confinement provided by the spiral reinforcement significantly increases the strain-ductility of the masonry prisms. This section focuses on the analytical evaluation of the ultimate strength and its corresponding longitudinal strain for confined masonry prisms. The concept of confined concrete was first introduced by Paulay and Priestley (1992), who provided pioneering analytical frameworks for understanding the effects of lateral confinement on compressive strength and ductility. Although originally developed for reinforced concrete elements, the underlying mechanism—lateral confinement improving ductility and ultimate strain—closely parallels that observed in the self-reinforced (SR) masonry blocks. The confinement in SR-blocks acts in a similar manner to transverse reinforcement in reinforced concrete, effectively delaying the onset of crushing and increasing the usable strain capacity.The effectiveness of two models from the existing literature, originally developed for concrete confined by spirals, is examined. The first model involves an empirical expression to determine the ultimate strength (MacGregor, et al. (2004)). This model can be used for concrete masonry with some considerations, using the following expressions:

$$f'_{cm} = f'_m + k_1 f_l \tag{2}$$

$$\varepsilon_{cm} = \varepsilon_m \left(1 + k_2 f_l / f'_m\right) \tag{3}$$

where, f'_m and ε_m are the specific compressive strength and its corresponding strain for the unconfined masonry prism. The parameters f'_{cm} and ε_{cm} represent the ultimate strength and its corresponding strain for the confined masonry prism, respectively. The parameter f_l represents the lateral confining pressure developed by the spiral reinforcement embedded in the SR blocks. The coefficients $k_1$and k_2 are functions of the concrete mix and the lateral confining pressure. The value of f'_m based on the Canadian Standard, evaluated in the previous section, is presented in Table 9.

Figure 10a illustrates the geometric characteristics of the spiral reinforcement used to manufacture the SR blocks in this study. The confining pressure, f_l, is a function of the diameter of the confining device, d_{cd}, and pitch, S_{cd}, of the spiral and the tensile yield strength, T_{cf}, of the steel wire that forms the spiral. Figure 10b shows how equilibrium is achieved between the forces when the spiral reinforcement provides lateral confinement.

Figure 11 shows the experimentally evaluated tensile stress-strain curves obtained for the steel wires of the spirals. The average tensile yield stress of the steel wire was evaluated to be f_y = 215

MPa. Given a wire diameter of 2.2 mm (cross-sectional area, A_S= 3.46 mm^2), its yield strength reads T_{cf}= 816.8 N. Referring to Figure 10b, based on the equilibrium of forces acting on the spiral, the confining pressure was obtained as $f_l = \frac{2T_{cf}}{d_{cd}S_{cd}}$ = 1.63 MPa.

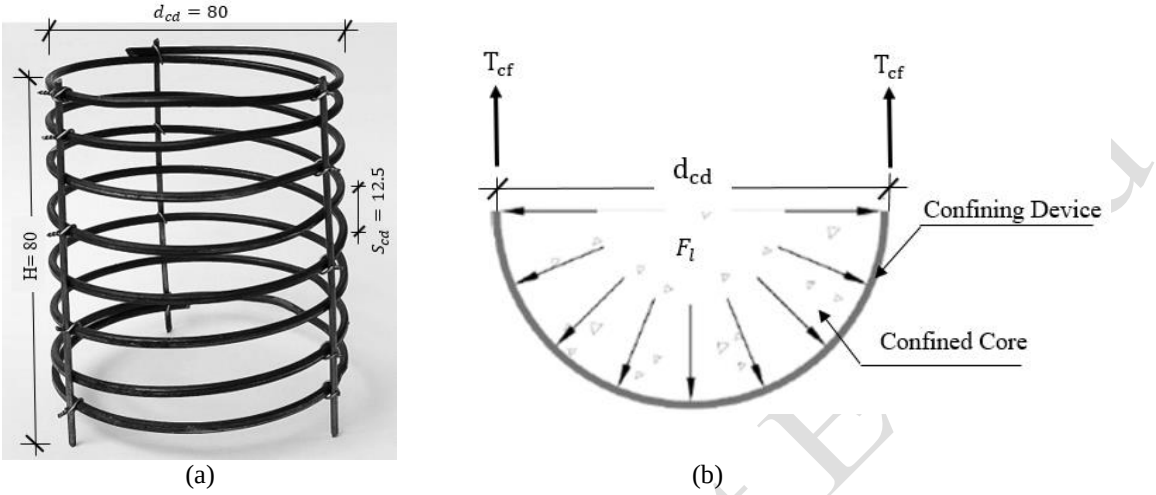

Fig 10. Spiral reinforcement as the confining device of SR blocks; a) Geometry (all dimensions in mm), b) Free-body diagram of forces

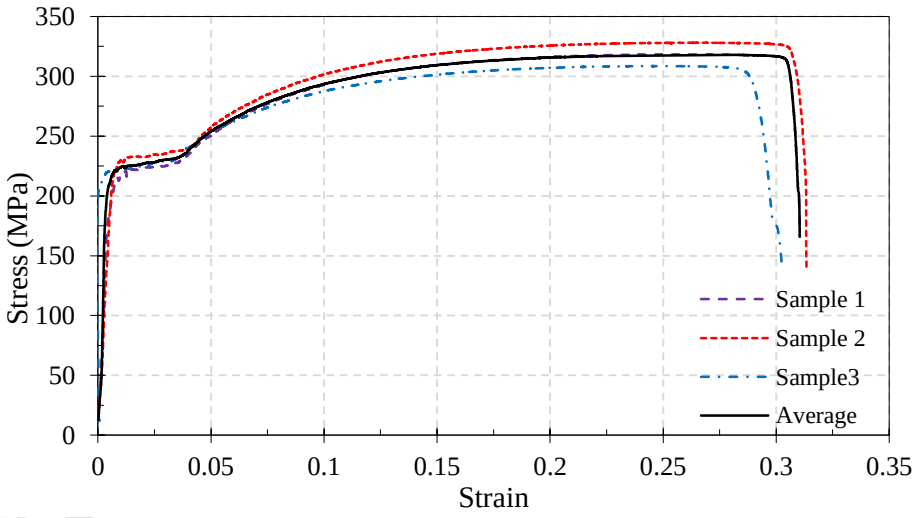

Fig. 11. Stress-strain behavior of the steel wire of the spiral reinforcement

The coefficients $k_1$and k_2 serves as a calibration factor to match the analytical with experimental strength evaluations. In a confined concrete column, depending on the concrete mix and the level of lateral confinement pressure provided by the spiral reinforcement, the average values for k_1 may range from 4.1 to 7 (Mander, et al. ((1988)). The constant coefficient of $k_1 = 4.1$ and $k_2 = 5k_1$, originally suggested for confined concrete . For the unconfined prisms, the peak strength was achieved at a strain of approximately $\varepsilon_m = 0.002$. Using Equation (3), ε_{cm} is evaluated to be 0.0082. According to the average stress-strain curve of the confined prisms shown in Figure 9, the maximum strength at the post-peak region of the curve, when the lateral confining pressure is in effect, was approximately 16.5 MPa, with a corresponding strain of 0.01. Therefore, for the

confined prisms in this study, Equation (3) underestimates ε_{cm} by approximately 18%. The ultimate strength of the masonry prism from Equation (2) is evaluated to be 17.78 MPa. When compared to the average experimental value, adjusted for aspect ratio effects (i.e., 0.96×16.5=15.84 MPa), it is evident that Model 1 overestimates the ultimate strength by 12.3%.

The second model used in this study to estimate the ultimate compressive strength of confined masonry prisms, f'_{cm}, and its corresponding strain, ε_{cm}, is a model that was originally developed for spiral-confined concrete by Paulay and Priestley and later formalized by Mander, Priestley, and Park (1988). In this study, it is adapted to predict the behavior of confined masonry prisms. The ultimate strength and corresponding strain are given by:

$$f'_{cm} = -1.254f'_m + 2.254\sqrt{{f'_m}^2 + 7.94f'_m f'_l} - 2f'_l \quad (4)$$

$$\varepsilon_{cm} = 0.002(1 + 5((f'_{cm}/f'_m) - 1)) \quad (5)$$

where, f'_l, the effective confining pressure applied to the core, can be evaluated as below.

$$f'_l = k_e f_l \quad (6)$$

In Equation (3) k_e is a coefficient that accounts for the effectiveness of the confinement that is defined as follows.

$$k_e = A_e/A_{cc} \quad (7)$$

In Equation (4) A_e is area of effectively confined concrete core and Parameter A_{cc} which is defined as area of core within center lines of perimeter spiral or hoops excluding area of longitudinal steel is evaluated as follows.

$$A_{cc} = A_c(1 - \rho_{cc}) \quad (8)$$

where, *Ac* is area of core of section within center lines of perimeter spiral and ρ_{cc} is ratio of area of longitudinal reinforcement to area of core of section. Therefore, from Eq. 6, the confinement effectiveness coefficient is for circular spirals

$$k_e = (1 - s_{cd}/2d_{cd})/(1 - \rho_{cc}) \quad (9)$$

Based on Fig10a, the spiral pitch and diameter are 12.5 mm and 80 mm, respectively. Since there are no longitudinal bars in the confined cores, ρ_{cc}=0, resulting in an effective confinement factor of $k_e = 0.93$. Using Equation (4), the ultimate strength of confined masonry prisms is estimated to be 19.2 MPa, which overestimates the average experimental value for the confined prisms in this study by over 21%. The corresponding strain ε_{cm}, evaluated from Equation (5) is 0.0092 that underestimates by approximately 7%. (Figure 9).

Table 10 presents the ultimate strength values (f'_{cm}) and their corresponding longitudinal strains (ε_{cm}) estimated for the confined versions of reference Prisms 1 to 3, based on Models 1 and 2 discussed in this section. The table also includes the average experimental compressive strength value obtained for the confined prisms. The experimental strength values in Table 10 have been adjusted using aspect ratio correction factor of 0.96, as specified by CSA-S304.1. The strength values in Table 10 represent the engineering stress of prisms, calculated by dividing the compressive force by the original cross-sectional area of the prism. Since the confined cores of the

masonry prisms included only 56% of their gross cross-section, the true ultimate stress resisted by the CP specimens is expected to be approximately 1.78 times the engineering ultimate stress values.

Table10 Analytical evaluation of the ultimate compressive strength of confined masonry prisms

Experimental*		Analytical			
		Model 1		Model 2	
f'_{cm}(MPa)	ε_{cm}	f'_{cm} (MPa) (error)	ε_{cm} (error)	f'_{cm} (MPa) (error)	ε_{cm} (error)
15.84	0.01	17.78 (+12.3%)	0.0082 (-18.0%)	19.2 (+21.2%)	0.0092 (-7.0%)

* The average experimental compressive strength has been adjusted for the aspect ratio of prism as per CSA-S304.1[22]

An examination of Table 10 indicates that, overall, Model 1 provides a more accurate estimation of the ultimate strength for the confined masonry prisms. The error of Model 1 in evaluating the ultimate strength of confined masonry is 12.3%, which is deemed satisfactory as it is less than the maximum coefficient of variation of 15% tolerated by many design codes, including CSA-S304.1 [24]. However, the model is not as accurate in evaluating ε_{cm}. The accuracy of Model 2, specifically in evaluating the ultimate strength f'_{cm} was found to be inadequate.

Figure 12 provides a direct comparison between the experimental results and the analytical predictions for both compressive strength and ultimate strain. The plot clearly shows that while both analytical models capture the general trend, they tend to overestimate the experimental ultimate strength values and underestimate the corresponding strain levels, confirming the need for model calibration for confined masonry.

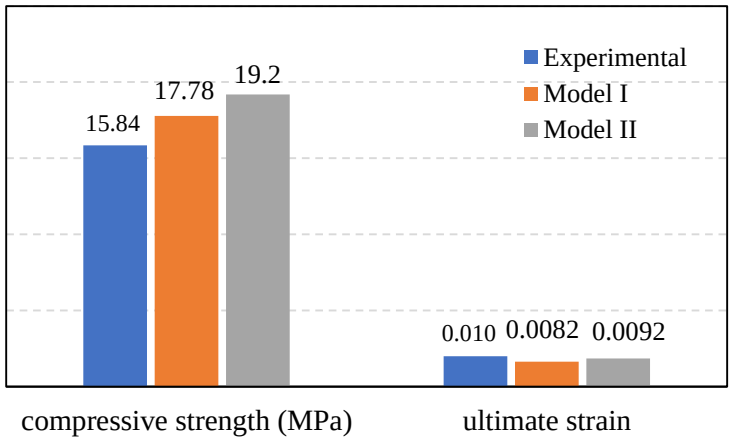

Fig. 12. Comparison between experimental results and analytical predictions for compressive strength and ultimate strain of SR-block masonry assemblies.

Models 1 and 2 were originally developed to predict the stress-strain behavior of confined concrete. The stress-strain curve in a confined masonry prism differs from that of confined

concrete (as discussed in Section 4.3). Additionally, the complex interaction between grout and concrete, as two distinct materials in the confined core of an SR-block, may result in different behavior compared to a confined concrete column. Therefore, neither of the two models investigated in this paper can be directly applied to confined masonry.

Model 1 relies on two constant coefficients, k1 and k2, which can be determined by calibrating it against a set of available experimental data. By fitting Model 1 (Equations (2) and (3)) to the ultimate strength (f'_{cm}) and its corresponding strain (ε_{cm}) values of the three confined prisms in this study (the circles shown in Figure 8), the average values of k1 and k2 were found to be 3.3 and 26, respectively. Using these coefficients, the ultimate strength and corresponding strain values were estimated to be 16.48 MPa and 0.0096, respectively. These estimates deviate by less than 5% from the average experimental data. However, the interim values obtained for k1 and k2 cannot yet be generalized to other masonry prisms due to the limited number of confined masonry prisms tested in this study. Further experimental data is required to achieve more representative k1 and k2 values for masonry prisms employing SR blocks.

6. SUMMARY AND CONCLUSIONS

The objective of this study was to experimentally investigate the effectiveness of novel self-reinforced (SR) concrete masonry blocks in enhancing the strain ductility and toughness modulus of masonry prisms. The SR blocks were composed of two adjacent circular hollow cells, each with internal spiral reinforcement. To achieve the research objectives, half-scale fully grouted masonry prisms were constructed using two types of blocks. The first type employed conventional stretcher blocks, termed unconfined prisms (UPs), whereas the second type utilized novel SR blocks, termed confined prisms (CPs). All measurements and materials were scaled down by a factor of ½, according to the similitude law.

The results of this study indicate that the application of SR blocks is effective in enhancing the deformation and mechanical properties of masonry prisms. The lateral confinement provided by the SR blocks in this study enabled the confined prisms to withstand very large strains with no significant loss of load capacity. The maximum strain of the unconfined prisms was slightly less than 0.3%, whereas the confined prisms retained approximately 80% of their initial peak capacity at the 2% strain limit. Moreover, the strain ductility and toughness modulus were found to be 5.2 and 7.9 times higher than those of the unconfined prisms, respectively.

The current code-based method for designing ductile masonry shear walls relies on the enhanced strain ductility of the masonry assemblage in the critical plastic hinge regions. SR-blocks offer a similar technical benefit by significantly increasing the ultimate compression strain of the masonry and potentially aiding in the construction of ductile shear walls.

Two analytical models available for predicting the ultimate strength and corresponding strain of confined concrete were evaluated and found not to be directly applicable to confined masonry. This is due to the complex interaction between grout and concrete in SR-blocks and the distinct stress-strain characteristics of confined masonry prisms, which differ from those in confined concrete columns. Further studies are required to explore the performance and benefits of employing SR blocks to improve the seismic responses of masonry structures.

ACKNOWLEDGMENTS

The authors acknowledge the financial support (Grant No. 97011048) provided by Iran National Science Foundation (INSF). They also express gratitude to the Razi University Research Laboratory for Structures and Materials for testing the specimens of this study.

Declaration of generative AI and AI-assisted technologies in the writing process

During the preparation of this work the authors used Grammarly in order to check grammar and refine the language to ensure clarity and precision in the manuscript. After using this tool, the authors reviewed and edited the content as needed and take full responsibility for the content of the publication.

REFERENCES

AbdelRahman, B.and Galal, K. (2021). "Monotonic and cyclic stress-strain models for confined concrete-masonry shear wall boundary elements". Engineering Structures**.** Volume 249, https://doi.org/10.1016/j.engstruct.2021.113343.

AbdelRahman, B. and Galal K, (2021). "Experimental investigation of axial compressive behavior of square and rectangular confined concrete-masonry structural wall boundary elements". Engineering Structures**.** Volume 243, https://doi.org/10.1016/j.engstruct.2021.112584.

Al-Ahdal, A., AbdelRahman, B. and Galal, K. (2025). "Compressive, shear, and tensile behaviours of concrete masonry: Experimental and numerical study". Construction and Building Materials. **458**: p. 139266. https://doi.org/10.1016/j.conbuildmat.2024.139266.

Albutainy M, Galal K. (2024). "Effect of boundary element detailing on the seismic performance of reinforced concrete masonry shear walls". Engineering Structures**.** Volume 300. https://doi.org/10.1016/j.engstruct.2023.117164

Aly, N. and Galal, K. (2019). "Seismic performance and height limits of ductile reinforced masonry shear wall buildings with boundary elements. Engineering Structures". **190**: p. 171-188. https://doi.org/10.1016/j.engstruct.2019.03.090

ASTM C1314. (2021). "Standard Test Method for Compressive Strength of Masonry Prisms". American Society for Testing and Materials. West Conshohocken, Pa.

ASTM C90. (2022). "Standard Specification for Loadbearing Concrete Masonry Units". American Society for Testing and Materials. West Conshohocken, Pa.

ASTM C1552. (2023). "Standard Practice for Capping Concrete Masonry Units, Related Units and Masonry Prisms for Compression Testing". American Society for Testing and Materials. West Conshohocken, Pa.

ASTM C144. (2018). "Standard Specification for Aggregate for Masonry Mortar". American Society for Testing and Materials. West Conshohocken, Pa.

ASTM C404. (2018). "Standard Specification for Aggregates for Masonry Grout". American Society for Testing and Materials. West Conshohocken, Pa.

ASTM C270. (2019). "Standard Specification for Mortar for Units Masonry". American Society for Testing and Materials. West Conshohocken, Pa.

ASTM, C 476 (2019). Standard Specification for Grout for Masonry. American Society for Testing and Materials. West Conshohocken, Pa.

ASTM C136. (2019). "Standard Test Method for Sieve Analysis of Fine and Coarse Aggregate". American Society for Testing and Materials. West Conshohocken, Pa.

Aşıkoğlu, A., Vasconcelos, G., Barontini, A., Lourenço, PB. (2025). "Quasi-static test on half-scale modern unreinforced masonry building with plan irregularity". Bulletin of Earthquake Engineering. 2025:1-43. 10.1007/s10518-025-02275-x

Banting BR. (2013). “Seismic Performance Quantification of Concrete Block Masonry Structural Walls with Confined Boundary Elements and Development of the Normal Strain-Adjusted Shear Strength Expression (NSSSE)”. Ph.D. Thesis, McMaster University, Hamilton, Canada

Chrysler J, (2022). Specifying Masonry Component Strength. Structure magazine.

CSA A179-14. (2014). “Mortar and grout for unit masonry”. Mississauga, Ontario, Canada: Canadian Standards Association.

CSA S304.1 (2014). “Design of masonry structures”. Mississauga, Ontario, Canada: Canadian Standards Association.

Drysdale R G, Hamid AA, (2005) “Masonry structures- behaviour and design”. First Canadian Edition. Canada Masonry Design Centre, Mississauga, ON, Canada.

Dou, M., Hsu, Y-C., Brzev, S. and Yang, T. (2022) “Stress–Strain Behaviour of Boundary Elements in Reinforced Block Masonry Shear Walls Under Uniaxial Compression”. Canadian Society of Civil Engineering Annual Conference: Springer. p. 171-87. DOI:10.1007/978-3-031-34027-7_12.

Islam, MM., Sen, D., and Chowdhury, SR. (2024). “Finite Element Analysis on The Effect of Gap Between Masonry Infill and Reinforced Concrete Frame Under Inplane Loading”. Civil Engineering Infrastructures Journal. DOI: 10.22059/ceij.2024.375383.2055

Gouda O. and Hassanein A. and Tarik Youssef, T., Galal, Kh. (2020). “Stress-Strain Behaviour of Masonry Prisms Constructed with Glass Fibre-Reinforced Grout”. Construction and Building Materials. https://doi.org/10.1016/j.conbuildmat.2020.120984.

Hart GC, Noland JL, Kingsley GR, Englekirkand R.E and Sajjad N.A. (1988). “The Use of Confinement Steel to Increase the Ductility in Reinforced Concrete Masonry Shear Walls”. The Masonry Society Journal, 7(2), T19-T42. https://masonrysociety.org/product/tms-ejournal-vol-7-no-2/

Harris, H.G. and Sabnis, G. (1999). “Structural modeling and experimental techniques”, CRC press.

Hervillard, T P C, (2005). “Effectiveness of Polymer Fibers for Improving the Ductility of Masonry Structures”. M.S. Thesis, Washington State University, Washington, U.S.A.

Joyal, M.P., Tait, M.J. and Drysdale, R.G. (2013). “Feasibility of Self-Reinforced Concrete Block for Improved Ductility”. 12th Canadian Masonry Symposium, Vancouver, Canada.

Kanani kashani, H., Shakiba, M., Bazli M., Hosseini M., Mortazavi M R. and Arashpour, M. (2023) “The structural response of masonry walls strengthened using prestressed near surface mounted GFRP bars under cyclic loading”. Materials and Structures. DOI:10.1617/s11527-023-02201-0

Kahrizi E., Aghayari R., Bahrami M. and Toopchi-Nezhad H., (2022). “On compressive stress-strain behavior of standard half-scale concrete masonry prisms”. Civil Engineering Infrastructures Journal. 10.22059/CEIJ.2022.324782.1758.

MacGregor, JG., Wight, JK. (2004). “Reinforced Concrete”: Mechanics and Design. 4 ed. Prentice Hall.

Mander, J., Priestley, M JN. and Park, R, (1988). “Theoretical Stress-Strain Model for Confined Concrete”. Journal of Structural Engineering, Vol. 114 (8), 1804-1826. https://doi.org/10.1061/(ASCE)0733-9445(1988)114:8(1804)

Niazi, E., Amin, F., Al Ismaeel, A., Chen, X., and Waqas, HA. (2025). “Sustainable seismic retrofitting of masonry walls using FRP composites: numerical analysis and parametric optimization”. Journal of Engineering and Applied Science. 2025;72:236. DOI:10.1186/s44147-025-00805-7

Paulay T, Priestley MJN, (1992) “Seismic Design of Reinforced Concrete and Masonry Buildings”. John Wiley & Sons, New York, USA.
Priestley MJN, Bridgeman DO., (1974). “Seismic Resistance of Masonry Walls”. Bulletin of the New Zealand National Society for Earthquake Engineering. 7(4), 167-187.

Paturova, A. (2006). “The Influence of Vertical Reinforcement and Lateral Confinement on the Axial Capacity of Masonry Block Walls”. M.S. Thesis, University of Saskatchewan, Saskatoon, Canada.

Raposo P., Furtado A., Arêde A., Varum H. and Rodrigues H. (2018). "Mechanical Characterization of Concrete Block Used on Infill Masonry Panels". International Journal of Structural Integrity Vol. 9 Issue 3 Pages 281-295. https://doi.org/10.1108/IJSI-05-2017-0030

SANZ (Standards Association of New Zealand). (2004). "Design of reinforced concrete masonry structures". NZS 4230. Wellington, New Zealand; 2004.

Snook, M K. (2005). "Effects of confinement reinforcement on the performance of masonry shear walls". Master of Science in Civil Engineering-Thesis, Washington State University, Washington, USA.

Shedid, M T., El-Dakhakhni, WW. And Drysdale RG. (2010). "Alternative Strategies to Enhance the Seismic Performance of Reinforced Concrete- Block Shear Wall Systems". J. Struct. Eng., 136(6), 676-689. https://doi.org/10.1061/(ASCE)ST.1943-541X.0000164

TMS 402/602. (2022). "Building Code Requirements and Specification for Masonry Structures". The Masonry Society, Pittsburgh, PA, USA.

Toopchi-Nezhad, H., Drysdale, RG. and Tait MJ. (2011). "Compression Behavior of Grouted Concrete Block Prisms Using Laterally Confined (Self-Reinforced) Concrete Block". Research Report, Deportment of Civil Engineering, McMaster University, Hamilton, Canada.